VISIBILITY FORECASTING FOR WARM AND COLD FOG CONDITIONS OBSERVED DURING FRAM FIELD PROJECTS

I.Gultepe[a;♦], P. Minnis[b], J. Milbrandt[c], S. G. Cober[a], G. A. Isaac[a], C. Flynn[d], L. Nguyen[b], and B. Hansen[a]

[a]Cloud Physics and Severe Weather Research Section,
Environment Canada, Toronto, Ontario, M3H 5T4, Canada
[b]NASA Langley Research Center, Hampton, VA 23681, USA
[c]Numerical Weather Prediction Research Section,
Environment Canada, Dorval, QC, H9P 1J3, Canada
[d]Pacific Northwest National Laboratory, Richland, WA 99352, USA

1. Introduction

Fog forms over various time and space scales under a variety of meteorological conditions. There have been many studies related to fog forecasting (Smirnova et al., 2000), remote sensing (Gultepe et al., 2007), and observations (Jacobs et al., 2007). Unfortunately, because of the difficulty in measuring fog microphysical parameters e.g., droplet number concentration (N_d), liquid water content (*LWC*), and effective radius (R_{eff}), the results from previous studies need to be reevaluated. These studies were related to mostly marine fog, radiation fog, and frontal fog conditions. Unfortunately, cold fog conditions (temperature T<0°C) have also not been studied in detail as much as warm fog conditions (Gultepe et al. 2007; Gultepe et al., 2008; Bott et al., 1990).

The Fog Remote Sensing and Modeling (FRAM) project was designed to focus on 1) development of microphysical parameterizations for numerical model applications, 2) development of remote sensing methods for fog detection, 3) understanding instrument capabilities and limitations for observations of fog and related parameters, and 4) integration of model and observation data for developing nowcasting applications. The main objective of this paper is to describe a research project on warm and cold fog conditions and visibility forecasting, and to summarize the results that have been obtained to date.

2. Observations

Surface observations during the FRAM field project were collected 1) at the Center for Atmospheric Research Experiment (CARE) site near Toronto, Ontario during the winter of 2005-2006 (Gultepe et al., 2008), 2) in Lunenburg, Nova Scotia during the summers of 2006 and 2007(Gultepe et al., 2008) and 3) at the Department of Energy (DOE) Atmospheric Radiation Measurement (ARM) Program at the North Slope Alaska (NSA) site, Barrow, Alaska during April of 2008 for the Indirect and Semi-Direct Aerosol Campaign (ISDAC) field program (called ISDAC-FRAM-B) (Gultepe et al., 2008). The main observations used in the analysis are fog droplet spectra from a fog measuring device (FMD; DMT Inc.), visibility (*Vis)* and precipitation rate (*PR*) from the VAISALA FD12P all-weather sensor and the OTT laser based optical disdrometer called ParSiVel (*Par*ticle *Si*ze and *Vel*ocity), and relative humidity with respect to water (RH_w) together with temperature (T) from the Campbell Scientific HMP45 sensor. Table 1 summaries the Environment Canada (EC) instruments available during the ISDAC-FRAM-B project that took place near Barrow, Alaska. Liquid water path (*LWP*) and liquid water content (*LWC*) were obtained from a microwave radiometer (MWR; Radiometric Inc.). Fog coverage and some microphysical parameters such as droplet size, phase, and LWP were also obtained from satellites e.g., such as GOES, NOAA, and Terra and Aqua MODIS products (Minnis et al., 2005). Note that not all instruments were available for each phase of the FRAM projects. Details on some of the instruments shown in Fig. 1 used for data collection during the ISDAC-FRAM-B can be found in Gultepe et al. (2007) and are discussed here briefly.

The FD12P Weather Sensor is a multi-variable sensor for automatic weather stations and airport weather observing systems (VAISALA Inc.). The sensor combines the functions of a forward scatter *Vis* meter and a present weather sensor. Figure 2 shows an example of FD12P measurements for the June 18 2006 case. This sensor also measures the accumulated amount and instantaneous *PR* for both liquid and solid precipitation, and provides the *Vis* and precipitation type related weather codes given in the World Meteorological Organization (WMO)

♦Corresponding Author: Dr. Ismail Gultepe, Environment Canada, Toronto, Ontario, Canada. email: ismail.gultepe@ec.gc.ca; Tel: 1-416-739-4607.

standard SYNOP and METAR messages. The FD12P detects precipitation droplets from rapid changes in the scatter signal. Based on the manufacturer's specifications, the accuracy of the FD12P measurements for *Vis* and *PR* are approximately 10% and 0.05 mm h^{-1} respectively. The fog-related microphysics parameters e.g. *LWC*, size, and droplet number concentration (N_d) were calculated from the FMD spectra for both liquid and ice clouds. Although an ice particle counter was available, its measurement size range is likely beyond the upper limit of the typical fog particle size, e.g., 50 µm. For subsaturated conditions, the Climatronics Aerosol Profiling (CAP) probe was used for measuring aerosol size and spectra between 0.3 and 10 µm. In saturated conditions, CAP measures the nucleated particles' characteristics.

The NOAA AVHRR (and/or GOES) observations were also available during FRAM projects, and some retrieval methods were used to detect fog conditions and its microphysics.

Table 1: Summarizes instruments available from the Environment Canada during ISDAC-FRAM-B.

Instrument	Measurement	Characteristics	FRAM-B/FRAM-L
(1) FMD fog monitor	Droplet/ice spectra	<50 µm	√/√
(2) CIP probe	Droplet/ice spectra	15-860 µm	NA√
(3) CAP aerosol	Droplet/aerosol spectra	0.3-10 µm; 8 channels	√/√
(4) OTT Distrometer	Droplet/ice particle spectra	400-25000 µm	√/Na
(5) YU IPC	Particle spectra	30-500 µm	√/Na
(6) FD12P vis	*Vis*/precip amount	0.1 mm/h	√/√
(7) Sentry Vis	*Vis*	>10 m	√/√
(8) DMIST Vis	*Vis*, images, and extinction		√/√
(9) YES TPS	Precip amount	0.25 mm/h	√/√
(10) VRG101	Precip amount	0.5 mm/h	√/√
(11) DSC111	Precip amount/friction	-	√/√
(12) DST111	Surface temperature	-	√/√
(13) SR50AT	Snow depth	-45 to 50°C	√/Na
(14) Eppley IR/SW	Broadband radiative fluxes	10%	√/√
(15) Campbell RH/T	RH and T	5% and 1°C uncertainty	√/√
(16) Young Ultra wind	3D wind and turbulence	4-32 Hz sampling rate	√/√
(17) SPN-1	Radiative flux, cloud cover	0.4-2.7 µm	√/Na
MWR TP3000	LWC, T, LWP, RH	-	√/√
Ceilometer	Backscatter, cloud base	-	√/√
ARM Lidar	Backscatter and Dep. ratio	-	√/Na

Fig. 1: Shows the instrument platform of the DOE ARM NSA site during ISDAC project.

3. Analysis and Results

The analyses are divided into four subsections and given below.

a. Warm fog microphysics

Warm fog conditions were observed very often during FRAM-L projects (~35% of time). In many cases, *Vis* dropped down to less than 100 m (Fig. 2). Here, a case study using observations from both ground-based instruments and satellites is summarized and a parameterization is developed.

Fig. 2: A marine fog event occurred over Lunenburg, NS, Canada on June 18 2006 during the FRAM-L field project.

Gultepe et al (2007) developed a parameterization for T>0°C and RH_w~100% that

is based on liquid water content (*LWC*) and droplet number concentration (N_d). The US current Rapid Update Cycle (RUC) model uses a *Vis-LWC* relationship for fog visibility (Smirnova et al. 2000; Stoelinga and Warner, 1999). Using information that *Vis* decreases with increasing N_d and *LWC,* a relationship between Vis_{obs} and $(LWC.N_d)^{-1}$ called the "*fog index*" is determined as

$$Vis_{obs} = \frac{1.002}{(LWC \cdot N_d)^{0.6473}} . \qquad (1)$$

This fit suggests that *Vis* is inversely related to both *LWC* and N_d. The maximum limiting *LWC* and N_d values used in the derivation of (1) are about 400 cm^{-3} and 0.5 g m^{-3}, respectively. The minimum limiting N_d and *LWC* values are 1 cm^{-3} and 0.005 g m^{-3}, respectively. In (1), N_d can be fixed as 100 cm^{-3} for marine environments and 200 cm^{-3} for continental fog conditions. These values of N_d, which were traditionally used in modeling applications, cannot be valid for all environmental conditions (Gultepe and Isaac, 2004). Examples of the fog microphysical characteristics for June 27, 2008 are shown in Fig. 3. Figures 3a, 3b, and 3c show *Vis* versus *LWC,* N_d, and *f(LWC;*N_d*),* respectively. Figure 3d shows the fog settling rate versus *f(LWC,* N_d*)* that can be used for model verification. Figure 3c suggests that *Vis* should be a function of both *LWC* and N_d, not only *LWC* as in forecasting models (Gultepe and Milbrandt, 2007)

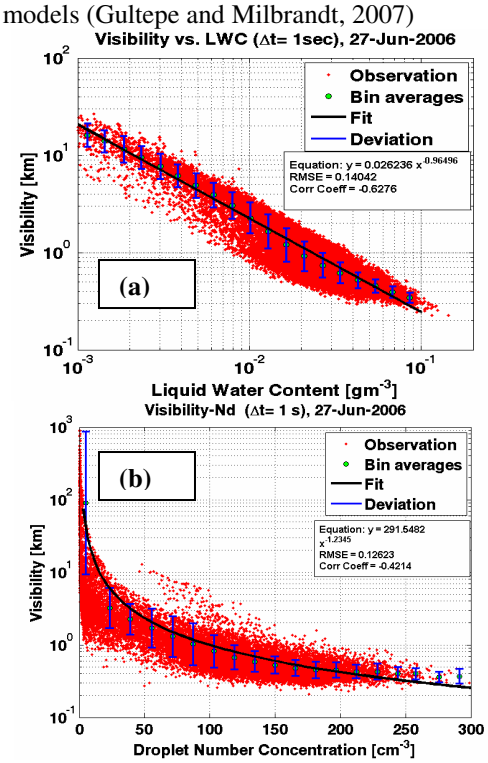

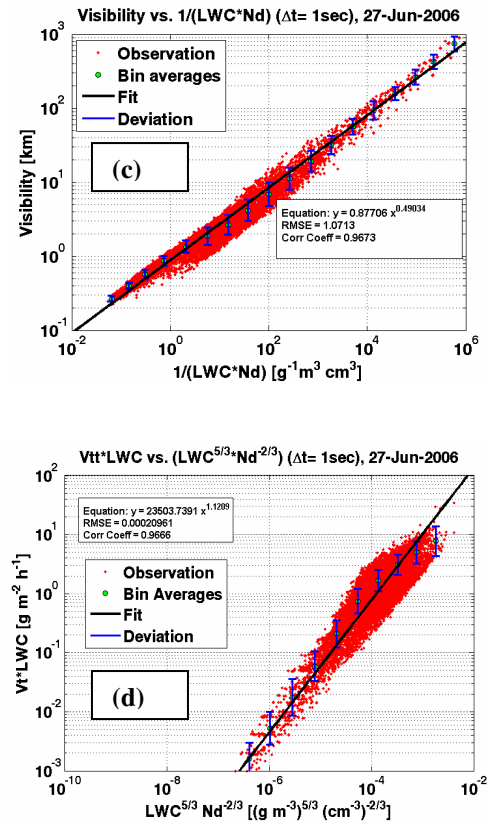

Fig. 3: Visibility function of *LWC* (a), N_d (b), and f(*LWC;*N_d) (c), and settling rate versus f(*LWC,* N_d) (d) on June 27 2006 for a warm fog event case.

b) Cold fog microphysics

The ice fog case during ISDAC-FRAM-B lasted 4 days from April 9 to April 12 2008 (Fig. 4). During this fog event, *Vis* decreased down to about 100 m and project flights were cancelled. Ice fog forecasting is usually not performed with forecasting models because ice water content (*IWC*) and ice crystal number concentration (N_i) are not accurately obtained from existing microphysics algorithms. If both parameters were available from a high-resolution fog/cloud model, they could be used for delineating ice fog regions and forecasting *Vis*. Ice fog occurs commonly in northern latitudes when *T* is below -15°C. The formation of ice fog usually develops when the *RH* becomes saturated with respect to ice (RH_i) without precipitation. Ice fog develops because of a deposition nucleation process that depends on nuclei size and concentration, and temperature.

Fig. 4: An ice fog event over Barrow, Alaska on April 10, 2008 during ISDAC-FRAM-B project.

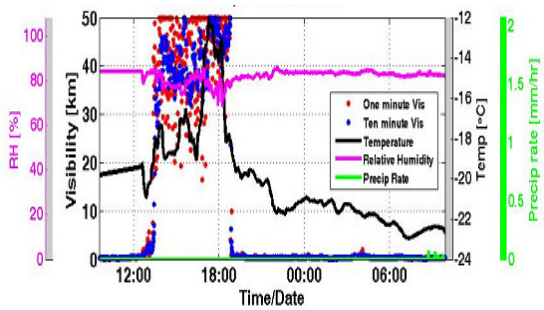

Fig. 5: Time series of relative humidity with respect to water (RH_w), *Vis*, temperature (*T*), and precipitation rate (*PR*) on April 10 2008 during ISDAC-FRAM-B.

Fig. 6: Frost formation over the IPC instrument during ice fog event on April 10 2008.

Time series of RH_w, *Vis*, *T*, and *PR* measured during April 10, 2008 during ISDAC-FRAM-B are shown in Fig. 5. This figure suggests that during the ice fog event, *Vis* was less than 100 m before 1200 UTC and after 1800 UTC during which no precipitation was observed. For this event, T<-20°C and RH_w was about 80% suggesting that these fog particles were composed entirely of ice. The ice fog event lasted from April 9 to April 12 during which the ISDAC aircraft flights were cancelled. Figure 6 shows a picture taken during the ice fog event at about 9 AM local time (18:00 UTC). This figure suggests that frost formation on the IPC counter (Table 1) was likely due to condensation of vapor and small ice particles at ice saturation conditions e.g., *RHi*=100%. During this event, several instruments were unable to collect accurate measurements.

Using aircraft observations collected during the First International Regional Experiment-Arctic Cloud Experiment (FIRE-ACE; Gultepe et al. 2008; 2003) found out that the frost point temperature (T_f) can be related to dew point temperature (T_d) as:

$$T_f = T_d + \Delta f \ , \qquad (2)$$

where T_d [°C] and T_f [°C] were obtained using LiCOR instrument humidity measurements (Gultepe et al., 2003) and their difference is parameterized as:

$$\Delta f = p_1 T_d^3 + p_2 T_d^2 + p_3 T_d^1 + p_4 \ , \qquad (3)$$

where p_1=0.000006; p_2= -0.0003; p_3=-0.1122; and p_4= 0.1802. If T_d is known, then T_f [°C] is calculated using. (2) and (3). The following equation is given for saturated vapor pressure by Murray (1967) as

$$e_s = 6.1078 \exp[\frac{a(T-273.16)}{(T-b)}], \qquad (4)$$

where T [K], e [mb], a=21.8745584 (17.2693882); b=7.66 (35.86) over the ice (water) surface. Then, using T_f and T, relative humidity with respect to ice (RH_i) is obtained from the following equation

$$RH_i = \frac{e_i(T_d + \Delta f)}{e_{si}(T)} \ . \qquad (5)$$

If RH_w and T are known, then T_d is calculated using an equation similar to (5) but for water. Using (2)-(5), RH_i is then calculated. If RH_i is greater than approximately 95%, T<-10°C, and no precipitation occurs, then ice fog regions can be obtained from a forecasting model. If Ice Water Content (*IWC*) is prognostically obtained, then *Vis* for ice fog, assuming that N_i and mean equivalent mass diameter (*d*) are known, can be calculated as (Ohtake and Huffman, 1969):

$$Vis = \frac{1}{3}\left[3.2\frac{IWC}{N_i}\right]^{1/3} - 1.5\bar{d} \ . \qquad (6)$$

Equation 6 shows how *Vis* changes with *IWC*, N_i, and *d*. In this work, it is suggested that N_i and *d* can be taken as 200 cm^{-3} and 7.2 µm (for high IWC e.g.>0.1 g m^{-3}), and as 80 cm^{-3} and 4.5 µm (for low *IWC*, e.g.,>0.01 g m^{-3}). If ice crystals form due to deposition of vapor directly onto ice nuclei at cold *T*, N_i can be parameterized as a

function of RH_i. A relationship between N_i and RH_i for ice fog has not been demonstrated. Note that (6) needs to be verified using measurements from the ISDAC-FRAM-B project. Preliminary results using FRAM-B observations as shown in Fig. 7 suggest the following relationship:

$$Vis = 0.242(IWC.N_i)^{-0.52} \qquad (7)$$

In this equation, Vis is indirectly correlated with the product of *IWC* and N_i that cannot be obtained from the 2DC optical probe measurements when ice crystal sizes<50 µm (Gultepe et al., 2001). This relationship needs to be further verified with additional observations.

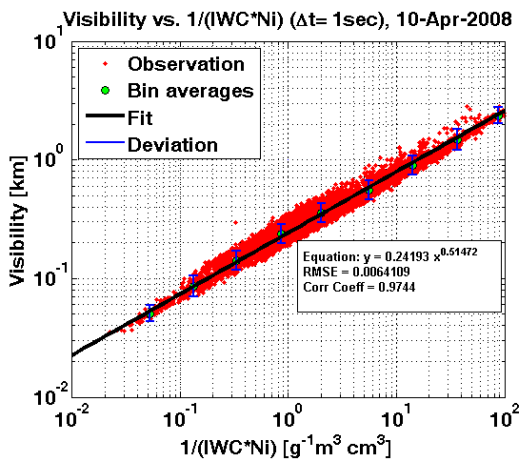

Fig. 7: Vis versus fog index (y-axis) based on observations collected during the April 10 2008 ice fog event from the ISDAC-FRAM-B project.

During the ice fog event (April 9-12), NOAA AVHRR images clearly indicated the region of ice fog coverage. The fog did not originate in the same manner as a warm fog because it occurred at T<-20°C and RHw~80% during which glazed ice was not observed over the instrument surfaces. On April 10 2008, the ARM MPL observations (Flynn et al., 2007) were available and used to confirm the ice fog occurrence. Figures 8a and 8b show the time-height cross section of uncalibrated attenuated aerosol backscatter ratio (β) and linear depolarization ratio (δ) measured by the ARM polarized MPL on April 10 2008, respectively. Figure 8a shows a very shallow fog layer below about 100 meters. This fog layer shows a high depolarization ratio in Fig. 8b as expected from ice fog. This is consistent with low RH_w values measured by chilled mirror hygrometers mounted at the four different levels along a meteorological tower (not shown) and with MWR measurements (not shown) showing negligible LWC during the fog event.

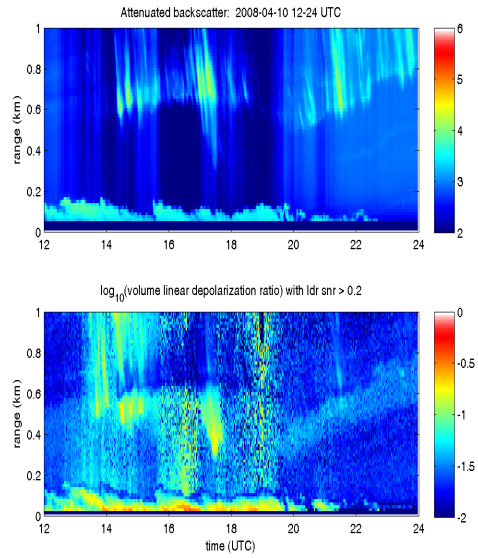

Fig. 8: Time-height cross section of the backscatter (β) and depolarization ratios (δ) from the ARM MPL during an ice fog event on April 10 2008.

c) Numerical fog forecasting

Visibility can be estimated by using parameters produced from detailed cloud schemes such as those available in the GEM model. Applying observation-based parameterizations (e.g., Eq. 1) as an alternative to those based on specific hydrometeor size distribution functions can be used to compute extinction coefficients directly. Researchers in Environment Canada are currently working on the implementation of a more detailed two-moment version of the cloud microphysics scheme (Milbrandt and Yau, 2005a; 2005b) to treat grid-scale clouds in the high-resolution version (2.5-km grid-spacing) of the GEM model. In this scheme, both *LWC* and N_d are independent prognostic variables. This will allow a more flexible application of the visibility parameterization of (1), without the restriction of prescribing a value of N_d. A simulation done using the GEM model to obtain *Vis* based on (1) is shown in Fig. 9. It suggests that improvements in the computed *Vis* estimates can be improved by 50% (Gultepe et al., 2007).

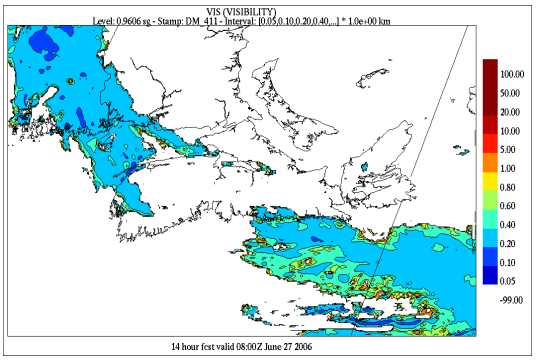

Fig. 9: Simulated warm fog event using (1) and a double moment microphysical scheme on June 27 2006. It was obtained using a GEM simulation based on a 14 hr forecast valid at 0600 UTC.

d) Satellite retrievals

The remote sensing study of the June 27 warm fog case is performed using 1) Terra MODIS satellite retrievals and 2) GOES and GEM model output work (Gultepe et al., 2007). The retrieval results suggest that integration of satellite observations with model output improved fog forecasting. The R_{eff} obtained from the MODIS observations of ~7 µm over the project site (not shown) were found to be comparable with the FMD measurements (Fig. 10) where median value of R_{eff} is estimated to be 6-8 µm. Figure 11 shows the warm fog area as detected using the integration of GOES observations and GEM model output. In this image, the model-based surface temperature and screen level *RH* were used in the integration of satellite observations. Gultepe et al. (2007) showed that inclusion of model output in the fog analysis together with satellite observations improved fog detection up to 30% of time.

During the April 10 2008 ice fog case, the NOAA AVHRR RGB image (Fig. 12) showed that ice fog covered a large area over the northern Alaska and Canada. It is optically thin as evident from the visibility of surface features underneath it. The ice fog conditions at the NSA site were characterized using surface observations. In this case, IWC reached to 0.2 g m^{-3} and *Vis* was less than about 100 m. Further analysis of this case using the retrieval techniques will help us to better detect the ice fog conditions in the northern latitudes.

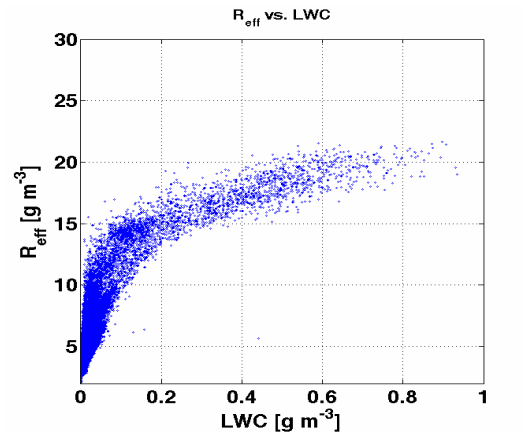

Fig. 10: Effective size (R_{eff}) versus *LWC* obtained from FMD measurements on June 27 2006.

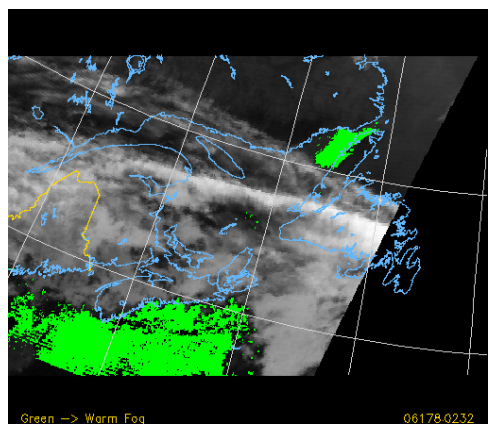

Fig. 11: A fog region obtained using GOES observations and GEM model output on June 27 2006.

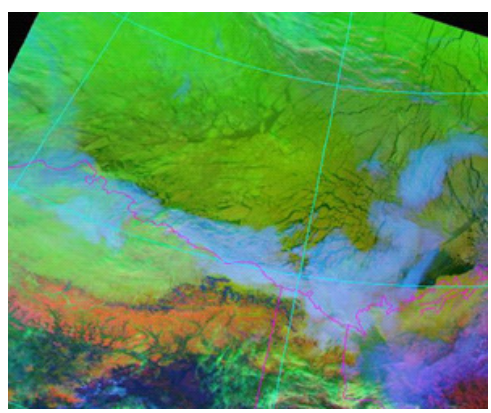

Fig. 12: The NOAA AVHRR RGB image of the ice fog event that occurred on April 10 2008 over the Barrow, Alaska. Ice fog regions are shown by light blue color.

5. Discussion

To accurately forecast/nowcast fog *Vis*, accurate model output parameters are required, e.g., *LWC,*

N_d, *RH*, and *PR*. If model output values for rain, snow, *RH*, and *LWC* are not accurate to better than 20-30%, the uncertainty in *Vis* can be more than 50% (Gultepe et al., 2006). If fog *LWC* and N_d are not accurately known from a model at the levels closest to the surface, then *Vis* based on other parameters e.g., such as *PR* or *RH*, or both, cannot be used to obtain accurate *Vis* values. Fog *LWC (or IWC)* and N_d *(or* N_i*)* are the major factors required for accurate *Vis* calculations and they should be obtained to an accuracy of about 10-20%. Figure 13 shows the measured *Vis* values from the FD12P and Sentry *Vis* sensors collected during an ice fog event over the ISDAC-FRAM-B project site. The *Vis* from the FD12P is comparable to the Sentry Vis sensor especially when *Vis* is less than 5 km. This suggests that for ice fog conditions both instruments can be used for *Vis* measurements when *Vis* is less than 5 km. For the higher *Vis* conditions, Sentry Vis values are found to be about 30% less than FD12P *Vis* values but opposite was true when light snow conditions existed during ISDAC project (not shown).

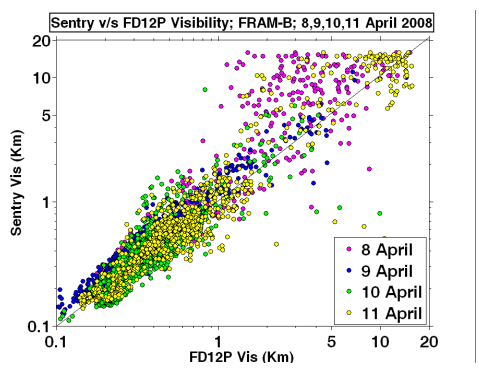

Fig. 13: Sentry Vis versus FD12P Vis values from an ice fog event over 4 days during ISDAC-FRAM-B field project.

The grid-point values of *Vis* obtained from the NWP models do not necessarily correspond directly to point measurements due to issues of model grid-spacing and spatial averaging. Model-based results should also consider sub-grid scale variability of *Vis, PR,* RH_w, and condensed water content.

Marine fog nowcasting/forecasting needs detailed surface fog measurements, high-resolution forecasting model outputs, and satellite observations. Integration of the data from various platforms can be used to obtain accurate fog *Vis*. As shown, satellite retrieved parameters integrated with model output can be very useful for improving fog forecasting skills. Over the Arctic regions, both satellite retrievals and microphysical parameterizations used in numerical models should be tested over various environmental conditions, e.g., over ice surface versus polynyas. To validate ice fog forecasting skills, lidar measurements can be useful for applications because they provide both δ and β, and the vertical extent of fog conditions.

6. Conclusions

The results from the GEM simulations suggest that the microphysics parameterization presented for warm fog, which includes N_d, can improve *Vis* values obtained from forecasting models. A new microphysical scheme to be used in the GEM limited area model (LAM) (Milbrandt and Yau, 2005a; 2005b) will provide both N_d and *LWC* values in a prognostic way that should lead to more accurate calculations of *Vis* values. The same analogy can also be applied for ice fog conditions.

For ice fog conditions, ice particle shape and size affect *Vis* as much as number concentration. Particle cross-sectional area (used in the calculation of extinction) of an ice crystal is related to particle habit, which affects *Vis* significantly. The combination of *IWC* and ice particle size (or N_i) can be used for *Vis* calculations if a particle shape is known accurately.

An ice fog visibility parameterization is suggested for model simulations of *Vis* at cold temperatures and an ice fog area coverage detection based on a new parameterization of RH_i to be used with numerical simulations is also proposed. These can be used in nowcasting/forecasting applications. A new equation is given for the frost point *T* calculation that can be used in RH_i calculation over a model grid area. The ice fog *Vis* parameterization (Ohtake and Huffman, 1967) needs to be verified and this will be done using the observations obtained during ISDAC-FRAM-B field project.

Remote sensing observations, including those from satellites and lidars data, can be effectively used for model validations and their integration together with surface observations will certainly increase the level of probability of accurate fog detection (Gultepe et al., 2007). Unfortunately, there are not enough statistics to develop detailed ice microphysical parameterizations to be used in

forecasting applications but a future ice fog project in Arctic will be performed to improve the data quality in ice fog conditions.

ACKNOWLEDGEMENTS

Funding for the FRAM project was provided by the Canadian National Search and Rescue Secretariat and Environment Canada. The authors are thankful to M. Wasey and R. Reed of Environment Canada for technical support. ISDAC was supported by the Office of Biological and Environmental Research of the U.S. Department of Energy through the Atmospheric Radiation Measurement (ARM) program and the ARM Aerial Vehicle Program with contributions from the DOE Atmospheric Sciences Program (ASP), Environment Canada and the National Research Council of Canada. Data were obtained from the ARM program archive, sponsored by the U.S. DOE, Office of Science, Office of Biological and Environmental Research, Environmental Sciences Division. The satellite analyses were supported by the ARM program and the NASA Advanced Satellite Aviation-weather Products (ASAP) Program.

REFERENCES

Benjamin, S. G., D. Dévényi, Stephen S. Weygandt, Kevin J. Brundage, John M. Brown, Georg A. Grell, Dongsoo Kim, Barry E. Schwartz, Tatiana G. Smirnova, Tracy Lorraine Smith, and Geoffrey S. Manikin 2004: An hourly assimilation/forecast cycle: The RUC, *Mon. Weather Rev.*, **132**, 495–518.

Bott, A., U. Sievers, and W. Zdunkowski, 1990: A radiation fog model with a detailed treatment of the interaction between radiative transfer and fog microphysics, *J. Atmos. Sci.*, **47**, 2153–2166.

Flynn, C.J., Mendoza, A., Zheng, Y., Mathur, S., 2007: Novel polarization-sensitive micropulse lidar measurement technique. Opt. Express, **15**, 2785-2789.

Gultepe, I., Pagowski, M., and Reid, J., 2007: Using surface data to validate a satellite based fog detection schem*, Weather and Forecasting,* **22,** 444-456.

Gultepe, I., S.G. Cober, G. Pearson J. A. Milbrandt B. Hansen, S. Platnick, P. Taylor, M. Gordon, J. P. Oakley, 2008: The fog remote sensing and modeling (FRAM) field project and preliminary results. *Bull. Amer. Meteor. Soc.*, submitted.

Gultepe, I., and J. A. Milbrandt, 2007: Microphysical observations and mesoscale model simulation of a warm fog case during FRAM project, *J. of Pure and Applied Geophy.***, 164**, 1161-1178.

Gultepe, I., M. D. Müller, and Z. Boybeyi, 2006: A new visibility parameterization for warm fog applications in numerical weather prediction models, *J. Appl. Meteor.* **45**, 1469-1480.

Gultepe, I., and G. Isaac, 2004: An analysis of cloud droplet number concentration (N_d) for climate studies: Emphasis on constant N_d, *Quart. J. Roy. Meteor. Soc.,* **130**, Part A, 2377-2390.

Gultepe, I., G. A. Isaac, and S. G. Cober, 2001: Ice crystal number concentration versus temperature for climate studies. *Inter. J. of Climatology*, **21**, 1281-1302.

Gultepe, I., G. Isaac, A. Williams, D. Marcotte, and K. Strawbridge, 2003: Turbulent heat fluxes over leads and polynyas and their effect on Arctic clouds during FIRE-ACE: Aircraft observations for April 199. *Atmosphere and Ocean,* **41(1)**, 15-34.

Jacobs, W., Vesa Nietosvaara, Andreas Bott, Jörg Bendix, Jan Cermak, Silas Chr. Michaelides, and Ismail Gultepe, 2007: COST Action 722, Earth System Science and Environmental Management, *Final report on Short Range Forecasting Methods of Fog, Visibility and Low Clouds.* Available from COST-722, European Science Foundation, 500 pp.

Milbrandt, J. A. and M. K. Yau, 2005a: A multimoment bulk microphysics parameterization. Part I: Analysis of the role of the spectral shape parameter. *J. Atmos. Sci.*, **62**, 3051-3064.

Milbrandt, J. A. and M. K. Yau, 2005b: A multimoment bulk microphysics parameterization. Part II: A proposed three-moment closure and scheme description. *J. Atmos. Sci.*, **62**, 3065-3081 (2005b).

Minnis, P., L. Nguyen, W. L. Smith, Jr., J. J. Murray, R. Palikonda, M. M. Khaiyer, D. A. Spangenberg, P. W. Heck, and Q. Z. Trepte, 2005: Near real-time satellite cloud products for nowcasting applications". *Proc. WWRP Symp. Nowcasting & Very Short Range Forecasting*, Toulouse, France, 5-9 September, CD-ROM 4.19.

Murray, F. W., 1967: On the computation of saturation vapor pressure. *J. App. Meteor.,* **6**, 203-204.

Ohtake, T. and P.J. Huffman, 1969: Visual Range in Ice Fog, *J. of App. Meteor.*, **8**, 499-501.

Smirnova, T.G., S.G. Benjamin, and J.M. Brown, 2000: Case study verification of RUC/MAPS fog and visibility forecasts. Preprints, 9th Conf. on Aviation, Range, and Aerospace Meteorology, AMS, Orlando, 31-36.

Stoelinga, M. T., and T. T. Warner, 1999: Nonhydrostatic, meso-beta scale model simulations of cloud ceiling and visibility for an east coast winter precipitation even. *J. Appl. Meteor.*, **38**, 385-4